Journal of Power Sources 194 (2009) 73–80

Contents lists available at ScienceDirect

Journal of Power Sources

journal homepage: www.elsevier.com/locate/jpowsour

Correlation between electrical properties and microstructure of nanocrystallized V_2O_5–P_2O_5 glasses

T.K. Pietrzak[a], J.E. Garbarczyk[a,*], I. Gorzkowska[b], M. Wasiucionek[a], J.L. Nowinski[a], S. Gierlotka[c], P. Jozwiak[a]

[a] Faculty of Physics, Warsaw University of Technology, Koszykowa 75, 00-662 Warsaw, Poland
[b] Faculty of Chemistry, Warsaw University of Technology, Noakowskiego 3, 00-664 Warsaw, Poland
[c] Institute of High Pressure Physics, Polish Academy of Sciences, Sokolowska 29/37, 01-142 Warsaw, Poland

ARTICLE INFO

Article history:
Received 24 October 2008
Received in revised form 10 February 2009
Accepted 10 February 2009
Available online 21 February 2009

Keywords:
Nanomaterials
Nanocrystallization
Cathode materials
Electronic conductivity
V_2O_5–P_2O_5 glasses

ABSTRACT

It was shown that by thermal nanocrystallization of a $90V_2O_5{\cdot}10P_2O_5$ glass one can obtain a novel nanomaterial exhibiting enhanced electronic conductivity. Using a combination of methods: DTA, SEM, XRD and impedance spectroscopy (IS), it was possible to find correlation between microstructure and electrical properties of the obtained material and to optimize conditions of its synthesis. The room temperature electronic conductivity of the nanocrystallized samples is $\sigma_{25} = 2 \times 10^{-3}$ S cm^{-1} and is by a factor of 25 higher than the conductivity of the as-received glass. The nanocrystallized material is thermally stable up to ca 400 °C, which is about 150 °C above the glass transition temperature of the original glass. Maximum electronic conductivity of the thermally treated samples reaches 2×10^{-1} S cm^{-1} at ca 400 °C. The activation energy for these samples (0.28 eV) are substantially lower than that found for the starting glass (0.34 eV). The experimental results were discussed in terms of a model proposed in this paper and based on a "core-shell" concept. The results obtained here can be important for the progress in the search of novel nanocrystalline cathode materials for applications in Li-ion batteries.

1. Introduction

Polycrystalline vanadium oxides, but also vanadophosphates (e.g. $VOPO_4$), because of their possibility of reversible intercalation of lithium and reasonable values of the electronic conductivity belong to a group of materials considered for cathodes in lithium-ion rechargeable batteries [1–3]. For years it has been known that also amorphous analogs of vanadium oxides (e.g. gels or glasses) exhibit similar or even better electrical and electrochemical properties than polycrystalline materials [4,5]. One of the key issues important for the progress in research on amorphous vanadate-based conductors is the enhancement of their electrical conductivity and improvement of the thermal stability. In recent years we have carried out research on conductive glasses including mixed electronic-ionic conductors of potential applications as cathode materials. During that period we have found out that some of those glasses (also vanadate–phosphate ones) relatively easily undergo nanocrystallization when subjected to an appropriate thermal treatment. Additionally such nanocrystallization has led to an increase in the electronic conductivity. Therefore we started systematic studies on conductivity enhancement of vanadate–phosphate glasses caused by thermal nanocrystallization [6–8]. The vanadate–phosphate glasses were chosen because the glass forming properties of V_2O_5 alone are insufficient to produce fully amorphous materials by a standard press-quenching process and it is necessary to add some amount of P_2O_5, a supporting glass former, to enhance glass forming properties of V_2O_5. The composition of the glasses studied in this work, set to $90V_2O_5{\cdot}10P_2O_5$, ensures reasonable electronic conductivity (due to high content of V_2O_5) and full amorphousness.

In this paper we have focused on optimization of heat treatment conditions required to achieve best conductivity enhancement of the samples and on correlations between temperature dependences of conductivity and microstructure, thermal events and other characteristics of thermal nanocrystallization phenomena occurring in the investigated glasses under various thermal treatment conditions.

2. Experimental

A series of vitreous vanadate–phosphate samples of the fixed composition $90V_2O_5{\cdot}10P_2O_5$ were prepared by a standard press quenching technique [7] adapted for this case. Appropriate amounts of pre-dried precursors: V_2O_5 (ABCR, 99.5%) and $(NH_4)H_2PO_4$

* Corresponding author. Tel.: +48 22 234 5350; fax: +48 22 628 2171.
E-mail address: garbar@if.pw.edu.pl (J.E. Garbarczyk).

0378-7753/$ – see front matter © 2009 Elsevier B.V. All rights reserved.
doi:10.1016/j.jpowsour.2009.02.031

(POCh – Polish Chemicals, 99.5%) were ground and mixed in a mortar. Alumina crucibles filled with the powders were placed in an electric furnace, heated to ca 950 °C in air, and held at the maximum temperature for 30 min. The molten mixtures were rapidly poured out onto a stainless-steel plate held at room temperature and immediately covered by another stainless-steel plate. The average thickness of the resulting samples was ca 0.7 mm. The amorphous state of all as-quenched samples was confirmed by powder X-ray diffractometry (XRD). XRD measurements were carried out using a Philips X'Pert Pro apparatus equipped with a $CuK_{\alpha 1}$ X-ray source and a Ni filter (λ = 1.54 Å). Thermal events taking place in the glasses upon heating were studied by differential thermal analysis (DTA). DTA runs were carried out for ground glass batches under argon from 20 to ca 600 °C at a set of heating rates ranging from 1 to 20 K min^{-1}. The temperatures of events detected on DTA traces were further used for planning temperature ranges of the electrical conductivity measurements carried out in heating–cooling cycles. The maximum temperatures and additional details of each of these cycles are given in the Section 3 of this paper. The electrical conductivity measurements were carried out using a system consisting of a Solartron 1260 Gain Phase/Impedance Analyzer integrated with a heater and modules of temperature programming and stabilization. All functions of the system (temperature programming, data acquisition etc.) were fully computer-controlled. The frequency range was 1 Hz–10 MHz, and the amplitude of the ac signal was 30 mV rms. Pilot measurements have shown that the impedance spectra of all samples under study were fragments of semicircles (less or more developed, depending on temperature). For all of them at frequencies below 1 kHz the impedance was purely ohmic with no dispersion, as expected for electronic conductors. Therefore the conductivity measurements were done at a fixed frequency of 100 Hz. In this way it was possible to carry out the experiment at relatively high effective heating rate, i.e. 1–2 K min^{-1}. This allowed to compare conductivity changes with thermal effects observed on DTA runs, taken at 1 K min^{-1} heating rate. Prior to these measurements gold electrodes were sputtered onto opposite faces of the samples using a Baltec SCD500 sputter coater. Microstructure of samples both as-received as well as subjected to heating–cooling cycles, was observed by field emission scanning electron microscopy (FE-SEM) using a LEO 1530 setup.

3. Results

3.1. DTA studies

Thermal stability of glasses can be effectively studied using thermal analyses in particular a DTA method. The DTA curves of a glass $90V_2O_5{\cdot}10P_2O_5$, taken at several heating rates (from 1 to 20 K min^{-1}) showed four thermal events: an endothermic baseline shift corresponding to a glass transition followed by three exothermic peaks (labeled A, B, C, respectively) related to crystallization processes (Fig. 1). Temperature values of these thermal events, lie in the following ranges: $225 \le T_g \le 250$ °C, $257 \le T_A \le 304$ °C, $307 \le T_B \le 333$ °C and $460 \le T_C \le 500$ °C. These temperatures obey a well-known empirical rule, which states that higher heating rates lead to higher temperatures of glass transition and crystallization. It should be noted that at the lowest heating rates (e.g. 1 K min^{-1}) the intensity of the peak B is weak and the peak C is almost negligible. On the other hand at high heating rates (20 K min^{-1}), peaks B and A start to overlap. The characteristic temperatures from Fig. 1 were used to analyze kinetics of non-isothermal crystallization of the glasses under study. The analysis was carried out on the basis of the Kissinger formula [9]:

$$\ln\left(\frac{\theta}{T_m^2}\right) = -\frac{Q}{k_B T_m} + C \quad (1)$$

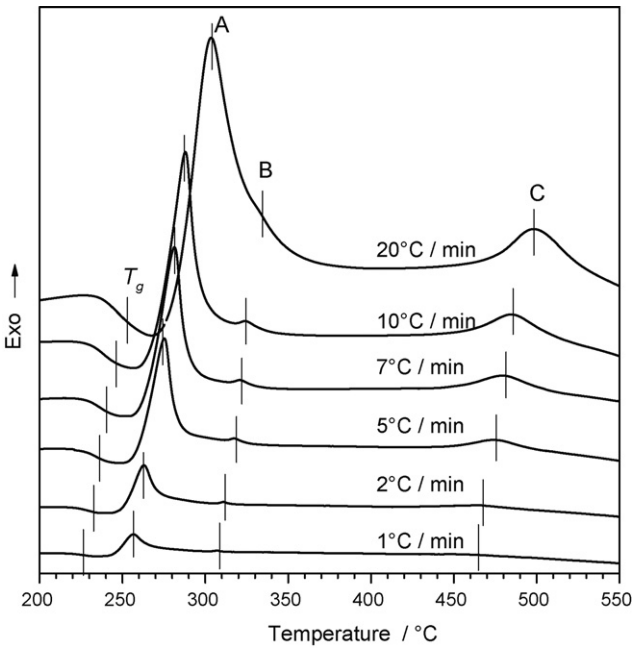

Fig. 1. DTA runs of $90V_2O_5{\cdot}10P_2O_5$ glasses at various heating rates.

where θ – heating rate, T_m – temperature of maximum of the crystallization peak, k_B – Boltzmann constant, Q – activation energy of the crystallization process and C – a constant.

The results of these analyses for peaks A, B and C (visible in Fig. 1) are plotted in Fig. 2. The numerical fitting of these dependences gave the following best fit values of the activation energy Q: 2.1 ± 0.2 and 1.3 ± 0.04 eV for the peak A, 4.2 ± 0.2 eV for peak B and 3.2 ± 0.2 eV for peak C. The presence of two activation energies of the dominating peak A may be due to two different processes: the higher value (2.1 eV) observed at low heating rates may reflect the formation of crystalline seeds (nucleation), while the other (1.3 eV) observed at higher heating rates can originate from the crystalline grains growth. The other crystallization peaks (B and C) are characterized by single activation energies. This suggests that these crystallization phenomena are single-step processes. It is worthy to note that the activation energy values of crystallization for the vanadate–phosphate glasses under study (1.3/4.2 eV) are substantially higher than those characteristic for the crystallization of fast ion conducting silver phosphate glasses (ca 0.81/1.86 eV) studied

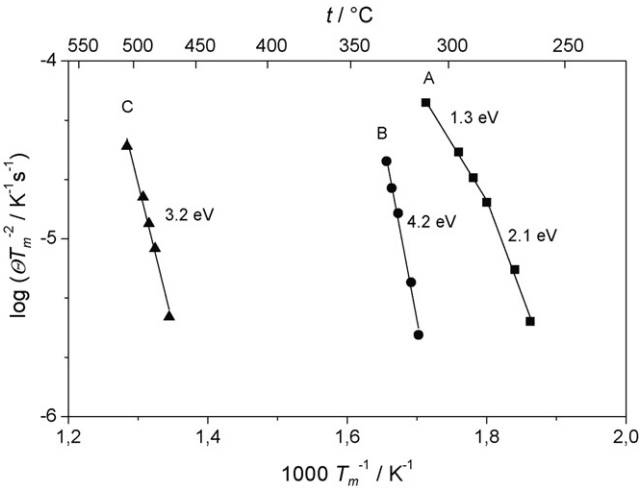

Fig. 2. Kissinger plots of crystallization peaks (A–C) for the $90V_2O_5{\cdot}10P_2O_5$ glass.

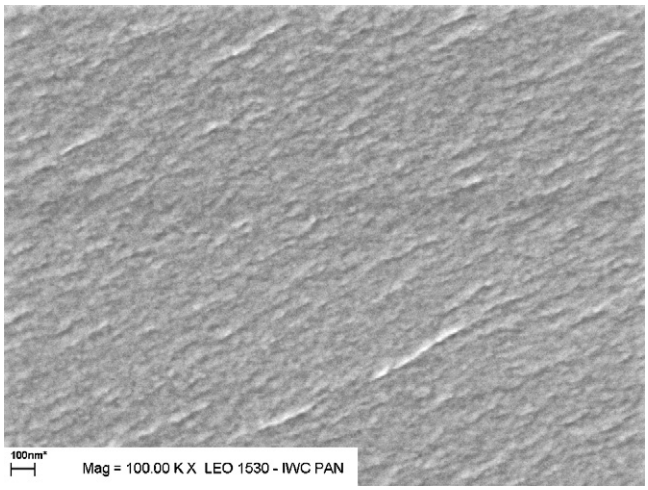

Fig. 3. SEM micrograph of the as received $90V_2O_5{\cdot}10P_2O_5$ glass.

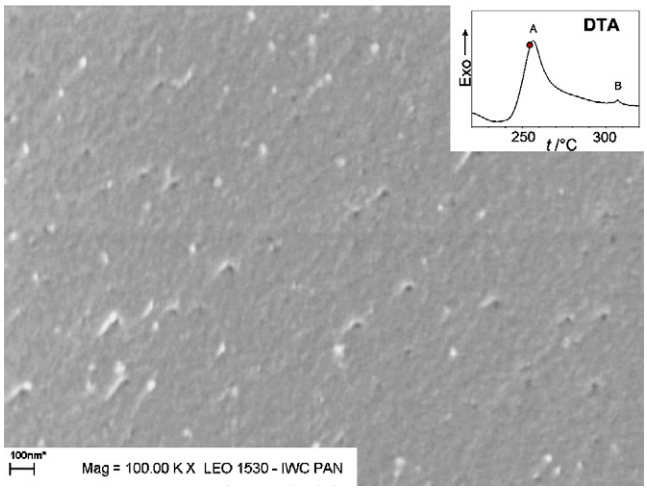

Fig. 5. SEM micrograph of $90V_2O_5{\cdot}10P_2O_5$ sample after its heating up to 255 °C (maximum of the crystallization peak A on a DTA curve shown in the inset).

by us earlier [10]. In the case of both glasses the values of the activation energies of crystallization are much higher than 0.2–0.4 eV, typical for their electronic [8] or ionic [10] conductivity.

3.2. SEM and XRD studies

As received samples under study were fully amorphous, as can be seen in a SEM micrograph and a XRD pattern shown in Figs. 3 and 4, respectively. The heating of the sample to 255 °C was followed by immediate cooling back to room temperature (Fig. 5). The temperature 255 °C was chosen intentionally as it corresponds to the maximum of the crystallization peak visible in the DTA curve taken at 1 K min^{-1} heating rate (inset in Fig. 5). Such a low heating rate is comparable to the rate of temperature increase in the electrical conductivity measurements. As can be seen in Fig. 5, a heating–cooling procedure with the maximum temperature of 255 °C does not lead to major changes of the microstructure except for some limited crystallization.

A different evolution of the microstructure can be observed after heating the sample to 275 °C, i.e. to temperature close to the end of the crystallization peak A (Fig. 6). In this figure one can see a number of small grains of sizes which vary within some limits, nevertheless vast majority of the grains are much smaller than 100 nm. The grains visible in Fig. 6 do not have regular shape, which should be expected if they were typical crystallites. At present it seems that smaller grains have tendency to form agglomerates and additionally that there is still a substantial fraction of the residual amorphous phase. More quantitative analysis concerning grain size distribution is presented below in the Section 4 of this paper.

A further modification of the microstructure (SEM micrograph shown in Fig. 7) took place after the annealing the sample at 360 °C, corresponding to a temperature above the crystallization peak B (inset in Fig. 7). Similarly to the case of samples heated up to 275 °C, also in this case one can see large featureless areas. However, contrary to the previous case (Fig. 6), the grains are more interconnected by a kind of amorphous medium. The shape of most of visible grains is not well defined, nevertheless when looking closer at the micrograph shown in Fig. 7, one can distinguish certain sharper, crystal-like resembling features in a number of these grains. The sample heated up to 360 °C is with no doubt crystalline as evidenced by its XRD pattern, taken after cooling the sample down to room temperature (Fig. 8). Vast majority of reflections seen in the pattern have been identified as corresponding to crystalline orthorhombic V_2O_5 (JCPDS card no. 41–1426). Fig. 9 presents a SEM micrograph of a sample heated up to temperature 550 °C. This temperature lies well above the crystallization peak C in DTA curve (inset in Fig. 9). Though the presence of the peak C is hardly observable in the DTA curve, nevertheless one can see a discernible deviation of the DTA baseline at 460 °C indicating that crystallization. The microstructure consists of well-developed crystallites with sharp edges and

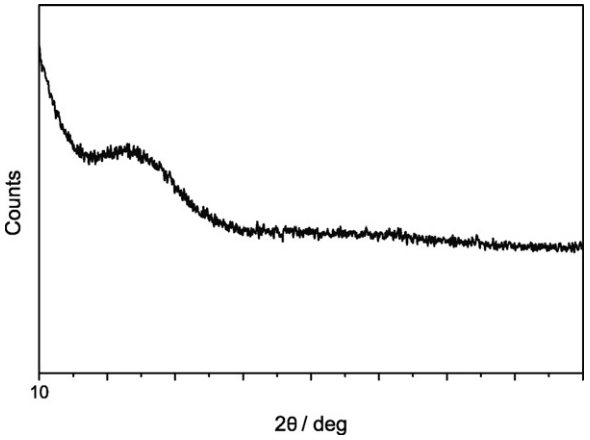

Fig. 4. XRD pattern of the as received $90V_2O_5{\cdot}10P_2O_5$ glass.

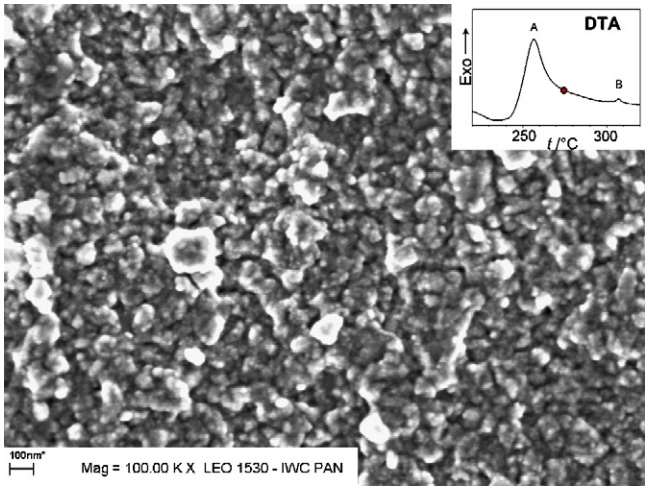

Fig. 6. SEM micrograph of $90V_2O_5{\cdot}10P_2O_5$ sample after its heating up to 275 °C (end of the crystallization peak A on the DTA curve shown in the inset).

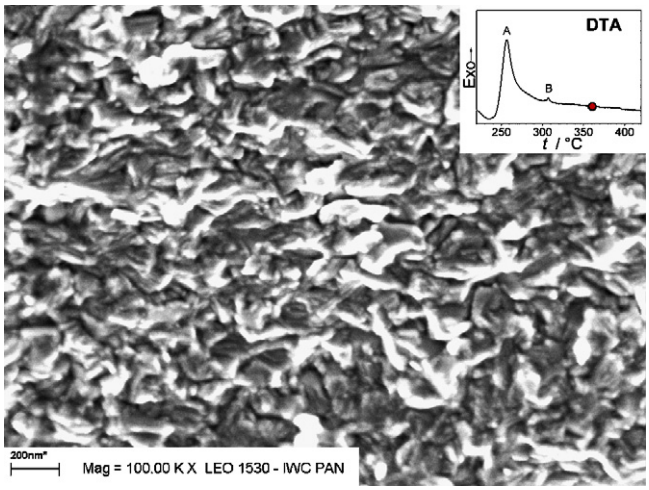

Fig. 7. SEM micrograph of $90V_2O_5{\cdot}10P_2O_5$ sample after its heating up to 360 °C (above the crystallization peak B on the DTA curve shown in the inset).

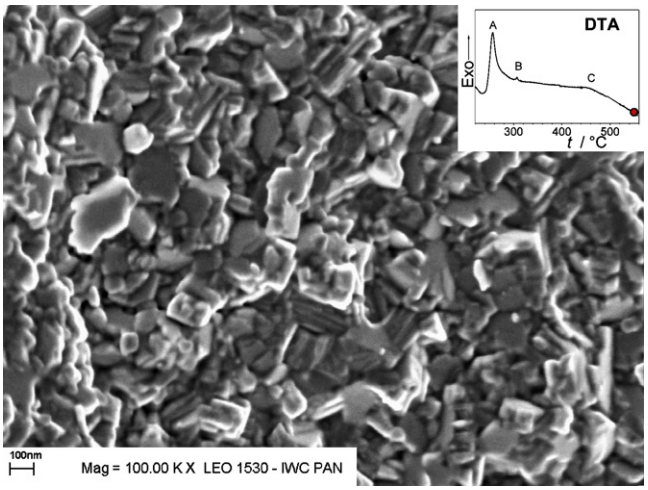

Fig. 9. SEM micrograph of a $90V_2O_5{\cdot}10\,P_2O_5$ sample after heating up to 550 °C (above the crystallization peak C on the DTA curve shown in the inset).

much more regular shapes. Besides small crystalline grains (below 100 nm) there are also large crystallites (above 200 nm). In Fig. 8, there is shown a comparison of three powder diffractograms of the glass $90V_2O_5{\cdot}10P_2O_5$ after its heating to 265, 360 and 550 °C, respectively. Further discussion of the heating conditions on an average size of the newly appearing crystallites will be included in the Section 4 of this article. Besides reflections originating from orthorhombic V_2O_5 there are several lines of a yet unidentified phase. The attempts to match these lines with the reflections of vanadia-, phosphate- or vanadophosphate-based structures collected in the JCPDS database, have failed so far.

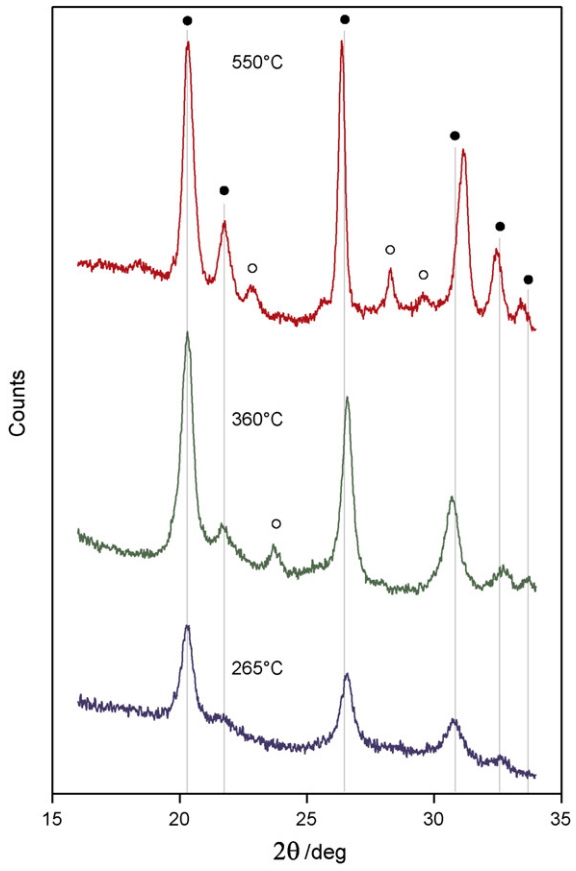

Fig. 8. XRD patterns of the samples after their heating up to T_{max} = 265, 360 and 550 °C. Solid circles correspond to orthorhombic V_2O_5 phase, open ones to an unidentified phase.

3.3. Electrical properties

3.3.1. Non-isothermal crystallization

As received glasses exhibit properties of amorphous semiconductors, in particular their electrical conductivity depends on temperature according to the Arrhenius formula: $\sigma T = \sigma_0 \exp(-E/kT)$, where E is the activation energy of the electronic conductivity. Fig. 10a presents the temperature dependences of the conductivity for the glass heated up to its glass transition temperature (T_g = 225 °C), and then cooled down to room temperature. As can be seen from this plot the conductivity values measured on cooling stage are identical with those measured on the heating. The activation energy values for heating and cooling runs are also identical (0.344 ± 0.002 eV). This means that the annealing of the glass under study below T_g does not induce any structural (or microstructural) modifications which could cause changes in the electrical properties. Discernible conductivity changes start only when the maximum temperature of the heating program exceeds crystallization temperature of the glass. In Fig. 10b, there are shown temperature dependences of the electrical conductivity of a sample heated up to 275 °C (which corresponds to the end of the crystallization peak A in the DTA trace presented in Fig. 1). To emphasize possible correlations between electrical conductivity and thermal events, the plot in Fig. 10b contains conductivity data together with a DTA curve. It should be reminded that the rate of temperature increase in the electrical conductivity measurements was comparable to the lowest of the heating rates of DTA measurements (1 K min^{-1}). The Arrhenius-like dependence with an activation energy E = 0.34 eV is observed up to ca 230 °C, i.e. close to T_g. At around the onset of crystallization peak A (ca 245 °C) the dependence of conductivity on temperature becomes non-Arrhenian. Microstructure of the sample annealed at 275 °C shown earlier (cf. Fig. 6) is nanocrystalline with the predominance of small grains (below 100 nm). Conductivity measured on the cooling run follows the Arrhenius formula with a single activation energy (E = 0.30 eV), which is lower than the activation energy measured during the heating stage (0.34 eV). What is characteristic for the cooling stage is that the electronic conductivity is much higher than that measured in the heating run.

For samples heated up to temperatures higher than 275 °C, one can observe the tendency to an increase in electrical conductivity caused by the heat treatment. A maximum extent of this tendency

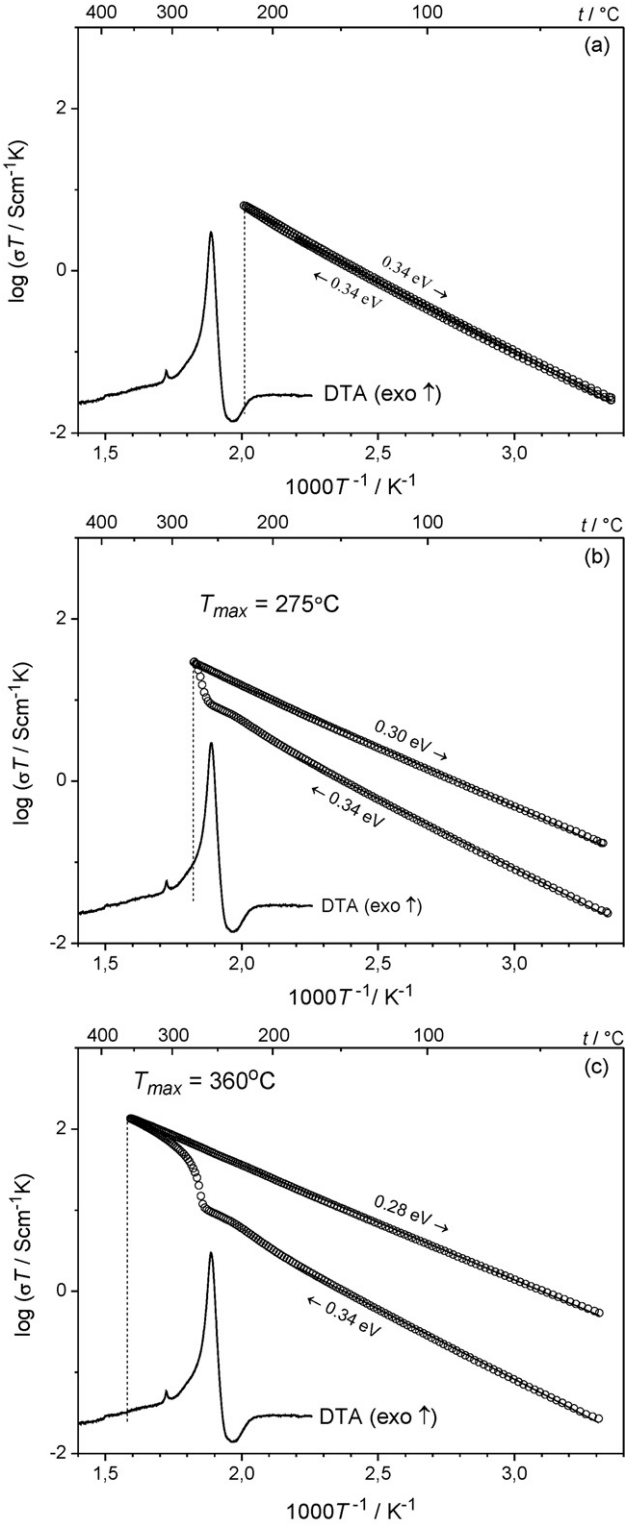

Fig. 10. Arrhenius plots of $90V_2O_5{\cdot}10P_2O_5$ glass: (a) heated up to glass transition temperature T_g and cooled down to room temperature, (b) heated up to 275 °C and cooled down to room temperature, and (c) heated up to 360 °C and cooled down to room temperature. A DTA curve taken on heating is shown for comparison.

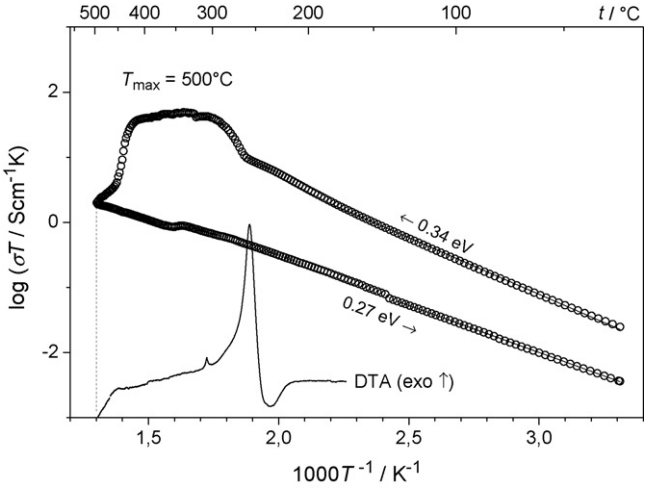

Fig. 11. Temperature dependence of conductivity for $90V_2O_5{\cdot}10P_2O_5$ sample heated up to 500 °C and cooled down to room temperature (a DTA curve taken on heating is shown for comparison).

was found for heating–cooling cycles with the upper temperature limit close to 400 °C. In Fig. 10c, there are shown temperature dependences of conductivity for the sample heated up to 360 °C and cooled down to room temperature together with the DTA curve on heating. It has been observed that the activation energy value and conductivity changes due to the heating are more pronounced that in the case of a cycle reaching maximum temperature of 275 °C. The activation energy measured on cooling was equal to 0.28 eV. The room temperature conductivity after the heating–cooling cycle was $\sigma_{25\,^\circ C} \approx 2 \times 10^{-3}$ S cm^{-1}, i.e. was much higher than 8×10^{-5} S cm^{-1} for the fully amorphous material before the cycle. The maximum conductivity in this cycle reached value of 2×10^{-1} S cm^{-1} at 360 °C. The primary cause of the positive conductivity changes caused by thermal treatment is the modification of microstructure (cf. Fig. 7). Thermally induced formation of many small grains leads to appearance of interfacial disordered regions between surfaces of these grains and the bulk of the amorphous phase. An important advantage of nanocrystallization is a remarkable increase in the thermal stability threshold of the obtained nanomaterial. As can be seen in Fig. 10c, the as-received glass is stable up to $T_g \approx 225$ °C, whereas the nanocrystallized sample is stable up to at least 360 °C. When the maximum temperature of the heating–cooling cycle is very high (>460 °C), higher than temperatures of crystallization processes seen in DTA curves, the conductivity decreases sharply which is shown in Fig. 11. In the SEM micrograph of a sample heated up to 550 °C (Fig. 9), it is clearly seen that the sample underwent complete massive crystallization resulting in well shaped crystallites. It is somewhat unexpected that despite a conductivity drop in this cycle the activation energy of conductivity in the cooling stage remains low. A probable reason is that on a local scale the transport mechanism in crystallized samples is the same as in the case of aforementioned samples heated to lower maximum temperatures (≤400 °C). Materials in all these cases contain some amount of defective well conducting regions around newly formed grains. All of these regions have a similar structure and conductive properties, which corresponds to similar activation energy. The difference lies in the volume fraction of these regions. In samples heated to lower temperatures (≤400 °C) it is relatively high, and in samples heated up to over 500 °C, it is substantially lower. This difference leads to a decrease of absolute values of conductivity in the latter case, but keeps the same activation energy in both situations.

3.3.2. Isothermal crystallization. Stability of the obtained nanomaterials

Apart from studies on non-isothermal processes affecting the microstructure and electrical conductivity of the samples (presented in Section 3.3.1) it is equally important to study the consequences of isothermal annealing. Fig. 12 shows two temperature

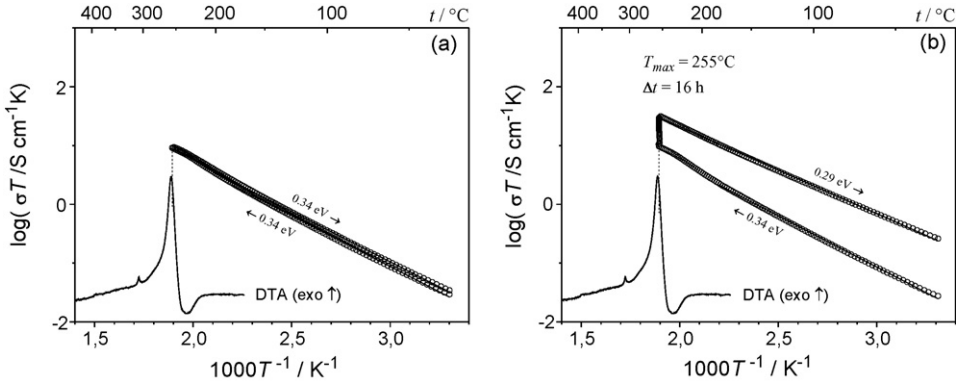

Fig. 12. Temperature dependences of conductivity for $90V_2O_5{\cdot}10P_2O_5$ sample: (a) heated up to 255 °C and immediately cooled down to room temperature, and (b) annealed at 255 °C for 16 h and cooled down.

dependences of conductivity for the same composition ($90V_2O_5\,10P_2O_5$) and temperature range (T_{max} = 255 °C). The difference between two data sets lies in the duration of the isothermal annealing at the maximum temperature. In one case in Fig. 12a, this duration was negligible (the cooling stage immediately succeeded the heating one) while in the other case there (data set (b) in Fig. 12) was a period of Δt = 16 h of annealing at the maximum temperature (255 °C) before the sample was cooled down to room temperature. There is a distinct difference between these two cases, both in absolute values of conductivity (higher for the annealed sample) and the activation energy (lower for the annealed sample). The experimental time dependence of conductivity for the annealed sample during its period of isothermal annealing at 255 °C is given in Fig. 13. Time t = 0 marking the beginning of the isothermal annealing usually does not correspond to the start of the isothermal crystallization [11]. For times from ca 100 min on, it was possible to fit the experimental data with a function:

$$\sigma(t) = \sigma_n \left[1 - \exp\left(-\left(\frac{t - t_0}{\tau}\right)^n\right)\right]^{2/3}. \quad (2)$$

The best fit parameters were: $\sigma_n = 6.8 \times 10^{-2}$ S cm^{-1}, τ = 4.6 h, n = 0.28 and t_0 = 1.1 h.

The exponent 2/3 in Eq. (2) was proposed to account dimensionality of the newly formed quasi-2D regions exhibiting enhanced conductivity. More details on Eq. (2) are given in the Section 4. Eq. (2) was derived from the classical Avrami formula for time dependence of isothermal crystallization [12]:

$$F(t) = 1 - \exp(-Kt^n), \quad (3)$$

where $F(t)$ – the volume fraction undergoing transition from amorphous to crystalline phase, K, n – constants.

An analogous experiment aiming at finding the effect of long-term annealing at the maximum temperature on the conductivity was done in the heating–cooling cycle reaching the highest temperature of 295 °C. There were two runs (the one, in which a sample heated up to 295 °C was without a delay cooled down and the other, in which sample was held at 295 °C for 18 h, before being cooled down. In this case, in opposition to the previous one the annealing did not cause any change of the conductivity and in both cases the temperature dependence of conductivity on cooling was the same for non-annealed and annealed sample. In both cases the activation energy values were almost identical (0.278 ± 0.002 eV for the non-annealed and 0.279 ± 0.002 eV for the annealed sample). It means that the isothermal annealing at 295 °C does not have any effect on the conductivity (contrary to the case of the annealing at 255 °C).

Similar reproducibility of the conductivity dependences and stability of its values was found for samples annealed at 340 °C. A nanocrystallized sample, after cooling down to room temperature, was heated up again to 340 °C and once more cooled down to room temperature. In all those cases conductivity values at corresponding temperatures and activation energies (0.28 eV) were the same.

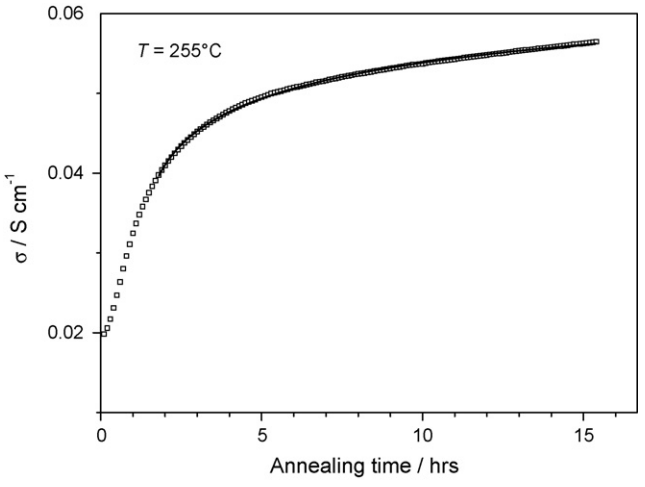

Fig. 13. Time dependence of electronic conductivity for the sample annealed at 255 °C for 16 h (the effect of isothermal nanocrystallization).

4. Discussion

Results of the conductivity measurements of as-received and thermally processed samples are summarized in Fig. 14 and Table 1.

Table 1
The dependence of conductivity σ_n (at 25 °C) and activation energy E for nanocrystallized glasses on the temperature T_{max} of the thermal treatment runs (σ_g denotes reference conductivity of as-received glass at 25 °C).

T_{max}/°C	E/eV*	$\sigma_n/10^{-5}$ S cm^{-1}	σ_n/σ_g
225	0.346	8.6	1.1
245	0.342	9.5	1.2
265	0.312	35	4.4
275	0.295	54	6.8
288	0.293	96	12.0
297	0.278	112	13.9
310	0.285	116	14.6
320	0.287	122	15.2
330	0.281	138	17.2
340	0.284	158	19.7
360	0.281	166	20.7
380	0.259	188	23.5
420	0.264	198	24.8

* With accuracy of ± 0.002 eV.

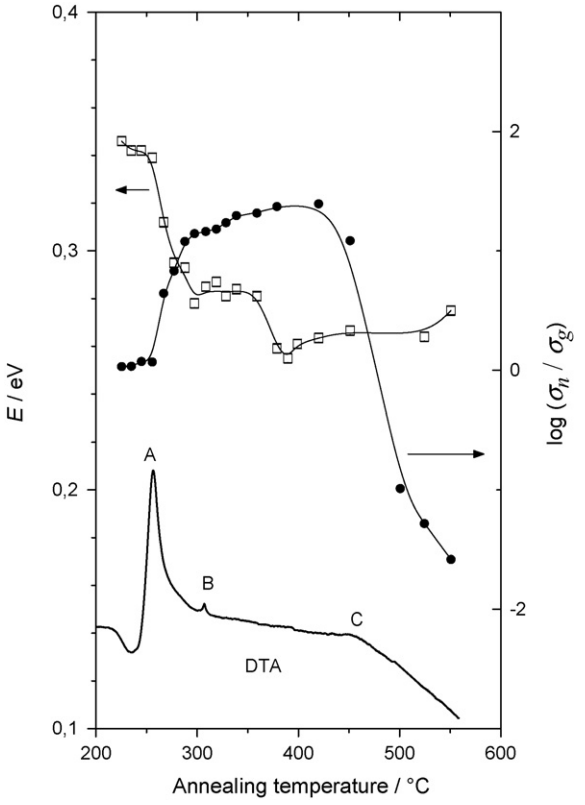

Fig. 14. Effect of thermal treatment on the electronic conductivity and the activation energy of the studied samples (lines are the guide to eyes only). The DTA heating run is included for comparison.

The data shown there represent ratio between room temperature conductivities (circles in Fig. 14) of thermally processed and as-received samples, and the activation energy values (squares) of the samples under study. The DTA curve inserted in Fig. 14 gives a comparative information about the thermal transitions taking place within the studied temperature range. It can be seen that the most pronounced increase in the conductivity, and a simultaneous decrease in the activation energy, occurs within the temperature range of crystallization peak A, in which a transformation from the glassy to nanocrystalline phase takes place. At temperatures above that range, values of both aforementioned quantities (a conductivity ratio and activation energy) become relatively stable, though above the crystallization peak B one can observe fluctuations of these parameters. Processing the samples at ca 400 °C leads to formation of nanomaterials exhibiting the highest electrical conductivity. When the temperature is higher than 460 °C samples undergo massive crystallization causing a decrease in conductivity.

For the interpretation of the experimental results it is useful to analyze average dimension of nanocrystalline grains in studied samples. That quantity was determined by two independent methods based on XRD and SEM studies (Section 3.2).

The mean size (averaged over volume) of the V_2O_5 crystallites, determined from broadening of the respective lines in the XRD pattern was estimated using the Scherrer formula:

$$\langle d\rangle_V^{XRD} = \frac{K\lambda}{\sqrt{\beta_0^2 - \beta_a^2}\cos\theta}, \quad (4)$$

where $K = 0.9$ (assumption of spherical grains), λ – wavelength of the incident XRD beam (here $\lambda_{CuK\alpha} = 1.54$ Å). Parameters β_0 and $\beta_a = 0.12^\circ$ correspond to full width of the given reflection at half maximum and the instrumental width, respectively.

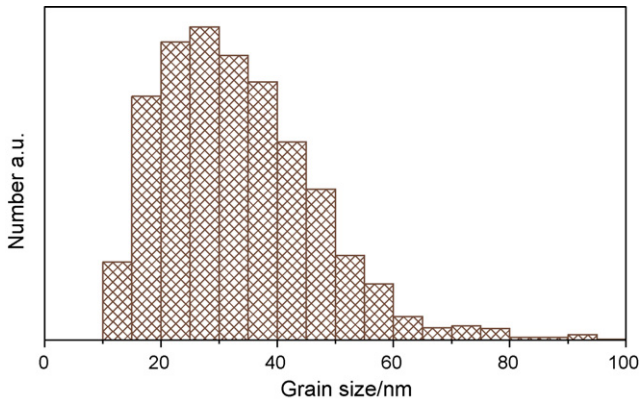

Fig. 15. A histogram of the grain size distribution determined from SEM micrographs taken for a sample heated up to 275 °C.

Estimations of average grain size $\langle d\rangle_V^{XRD}$ from line broadening of XRD patterns (Fig. 8), using the Scherrer formula (Eq. (4)) give the following values: 20 ± 2, 26 ± 3, and 46 ± 5 nm for samples heated up to 265, 360 and 550 °C, respectively. From the above sequence it is seen that the grain size is larger for higher annealing temperature, as one could expect.

To determine grain sizes by SEM method we used the specialized image processing software [13]. By applying that software to SEM micrograph in Fig. 6, it was possible to determine grain size distribution of a nanocrystallized sample (heated up to 275 °C). The corresponding histogram is shown in Fig. 15. It can be seen that the size of the majority of grains is in the 10/80 nm range. One has to be aware that by using the software [13] one obtains surface averages, whereas the XRD method yields volume averages. In order to compare both results correctly, a volume average for SEM method has to be calculated from surface averages as follows [14]:

$$\langle d\rangle_V^{SEM} = \frac{\langle d^2\rangle_S}{\langle d\rangle_S}, \quad (5)$$

where subscripts S and V denote surface and volume averages, respectively. Application of Eq. (5) to our SEM data gives $\langle d\rangle_V^{SEM} \approx 40$ nm.

Comparing a value of $\langle d\rangle_V^{SEM}$, corresponding to 275 °C, to values of $\langle d\rangle_V^{XRD}$, corresponding to 265–360 °C, one can notice that the former value is about twice as high as the latter one. Generally such a discrepancy may arise from a possibility that a grain seen by SEM is composed of several smaller crystallites. However in our case, from the SEM and conductivity data, it is more likely that a crystalline part of the grain (sensed by XRD) is enveloped by a strongly distorted or even amorphous one. The whole grain, with its crystalline inner part and distorted outer part is seen in SEM micrographs. This description is in line with a "core-shell" model of the nano-sized grains in thermally nanocrystallized materials such as the one under study. According to this model a grain consists of an inner fully crystalline "core" and an outer highly disordered, defective and non-stoichiometric "shell". The same "core-shell" concept can explain the conductivity enhancement caused by nanocrystallization. Fig. 16 shows a representation of such a model. The overlapping and intersecting defective shells around crystalline cores can form a complicated system of paths for facilitated electron transport. The mechanism of electronic transport in vanadium oxides consists in the small polaron hopping between aliovalent V^{4+} and V^{5+} sites. In the regions where the local concentration of the V^{4+}–V^{5+} pairs is high, the conductivity is also high. Such a situation takes place inside and around the defective grain-shell areas. The influence of the "interfacial" factor on the conductivity enhancement can be deduced from the good correlation between the increase in electrical conductivity during isothermal nanocrystallization (Eq. (2))

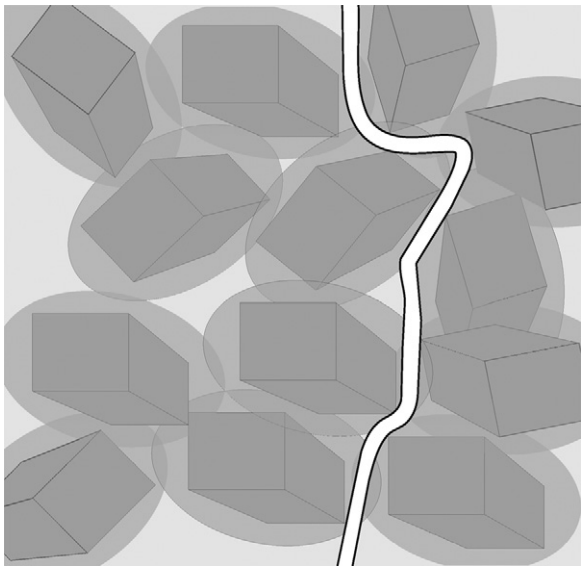

Fig. 16. A model of the easy conduction paths in studied nanomaterials using a "core-shell" concept.

and the progress in the isothermal nanocrystallization itself (represented by the Avrami equation (Eq. (3)). The important difference between Eqs. (2) and (3) is the exponent of 2/3 which is present in the expression in a parenthesis of Eq. (2) and is absent in Eq. (2). This exponent was introduced by us to the Eq. (2), because the well conducting interfacial regions formed during nanocrystallization have a quasi 2-dimensional character of shells around grains, while the progress in nanocrystallization described by the Avrami Eq. (3) describes the changes of the volume occupied by the newly formed crystallites. Therefore the exponent of 2/3 represents the ratio between the dimensionalities of the interfacial well conducting regions around grains (quasi 2D) and volume changes of the grains themselves (3D).

To explain the conductivity increase during nanocrystallization it is useful to refer to the well established Mott theory on electron hopping in disordered systems [15] and to adopt it to the case of nanocrystallized glasses. According to the Mott theory, the conductivity at temperature $T > \theta/2$ (half of the Debye temperature) is expressed by the formula:

$$\sigma = \frac{e^2 c(1-c)}{kRT} \nu_e e^{-2\alpha R} e^{-E_e/kT} = \sigma_{e0} e^{-E_e/kT}, \quad (6)$$

where R is the average distance between hopping centers, $\nu_e = \hbar/m_e R^2$, α is the inverse localization length of the electron wave function, $c = [V^{4+}]/([V^{4+}] + [V^{5+}])$ is the fraction of occupied hopping sites for electrons and E_e is the activation energy of electronic conduction. The theoretical expression for E_e includes a term $W = W_0(1 - r_p/R)$, where W_0 – a constant. A parameter r_p denotes a radius of a small polaron [15]. The Eq. (6) indicates that electronic conductivity is higher and an activation energy is lower when the distance R between hopping centers becomes smaller. In the case of samples under study it can be expected that due to nanocrystallization process the concentration of V^{4+}–V^{5+} pairs is higher near the surfaces of the newly formed crystallites than inside the crystallites. Higher number of neighboring V^{4+}/V^{5+} hopping centers in the interfacial regions leads to smaller average distance between the hopping centers, and consequently (cf. Eq. (6)) it causes an increase in conductivity.

For the samples heated up to temperature higher than ca 500 °C one observes massive crystallization, consisting in a considerable growth of the crystallites and the gradual disappearance of defective disordered regions covering crystalline cores of the nanocrystallites. In the case of massive crystallization the grains, visible in SEM micrographs (Fig. 9) become well developed crystallites with sharper edges and more regular shapes than the grains produced during nanocrystallization at lower temperatures. A negative consequence of the massive crystallization is the decay of the "easy conduction paths" of the interfacial regions and a conductivity drop (Fig. 14).

5. Conclusions

A new electronic conductive material was prepared by a thermal nanocrystallization of V_2O_5–P_2O_5 glasses. The conditions of its synthesis were optimized using a combination of DTA, XRD, SEM and impedance spectroscopy methods. The resulting nanomaterial exhibits promising properties. Thermal nanocrystallization leads to an increase in the electronic conductivity by a factor of 25, a decrease in the activation energy and an increase in thermal stability threshold by ca 150 °C, in comparison with the original glasses. A substantial improvement of the electrical properties of the synthesized conductors is most-likely related with highly disordered shells around V_2O_5 nanocrystalline cores. In these shells the concentration of V^{4+}–V^{5+} pairs is distinctly higher than in nanocrystalline cores. The disappearance of the disordered shells due to massive crystallization causes a considerable conductivity drop.

The described method of thermal nanocrystallization of a glassy phase can be used in the search and development of new nanocrystalline cathode materials for Li-ion batteries.

References

[1] M.S. Whittingham, Chem. Rev. 104 (2004) 4271–4301.
[2] C.P. Grey, N. Dupré, Chem. Rev. 104 (2004) 4493–4512.
[3] M. Wakihara, Mater. Sci. Eng. R33 (2001) 109–134.
[4] D.B. Le, S. Passerini, J. Guo, J. Ressler, B.B. Owens, W.H. Smyrl, J. Electrochem. Soc. 143 (1996) 2099–2104.
[5] C.H. Chung, J.D. Mackenzie, L. Murawski, J. Non-Cryst. Solids 32 (1979) 91–104.
[6] J.E. Garbarczyk, P. Jozwiak, M. Wasiucionek, J.L. Nowinski, Solid State Ionics 175 (2004) 691–694.
[7] J.E. Garbarczyk, P. Jozwiak, M. Wasiucionek, J.L. Nowinski, Solid State Ionics 177 (2006) 2585–2588.
[8] J.E. Garbarczyk, P. Jozwiak, M. Wasiucionek, J.L. Nowinski, J. Power Sources 173 (2007) 743–747.
[9] H.E. Kissinger, Anal. Chem. 29 (1957) 1702–1706.
[10] M. Mroczkowska, T. Czeppe, J.L. Nowinski, J.E. Garbarczyk, M. Wasiucionek, Solid State Ionics 179 (2008) 202–205.
[11] A.T. Lorenzo, M.L. Arnal, J. Albuerne, A.J. Mueller, Polym. Test. 26 (2007) 222–231.
[12] M. Avrami, J. Chem. Phys. 7 (1939) 1103–1112;
M. Avrami, J. Chem. Phys. 8 (1940) 212–224;
M. Avrami, J. Chem. Phys. 9 (1941) 177–184.
[13] ImageJ – http://rsbweb.nih.gov/ij.
[14] R.L. Snyder, J. Fiala, H.J. Bunge, Defect and Microstructure Analysis by Diffraction, Oxford University Press, Oxford, 2000.
[15] I.G. Austin, N.F. Mott, Adv. Phys. 50 (2001) 757–812.